Title
Femtosecond filament-laser ablation molecular isotopic spectrometry

Authors
Hou, Huaming
Chan, George C-Y
Mao, Xianglei
et al.

Publication Date
2015-11-01

DOI
10.1016/j.sab.2015.09.014

Peer reviewed

Femtosecond Filament-Laser Ablation Molecular Isotopic Spectrometry

HuamingHou[a,b], George C.-Y. Chan[a], XiangleiMao[a], RongerZheng[b], VassiliaZorba[a]and Richard E. Russo [a,*]

1. Lawrence Berkeley National Laboratory, Berkeley, CA 94720, USA
2. Ocean University of China, Qingdao, 266100, P. R. China

Abstract

A new remote sensing technology for real-time isotopic analysis is introduced:Femtosecond Filament-Induced Laser Ablation Molecular Isotopic Spectrometry (F^2-LAMIS).The technique combines femtosecond (fs) laser filamentation and ablation-based molecular isotopic spectroscopy,thereby enabling isotopic analysis of samples at a distance, in ambient air and at ambient pressure conditions.Isotopic analysis of zirconium (Zr) samples by F^2-LAMIS is demonstrated, and the molecular and atomic emission intensity, and properties of the filament-induced plasma generated at different filament propagation distanceswere investigated. Spectral fitting of F^2-LAMIS spectraenabledsemi-quantitative isotopic analysis without the use of calibration standards, whichwasindependent of the filament propagation distance for the studied range.This technology provides new capabilities for direct isotopic ratio measurements at remote distances.

Keywords: Femtosecond Filament-Induced Laser Ablation Molecular Isotopic Spectrometry (F^2-LAMIS); Isotopic Analysis; Laser Ablation Molecular Isotopic Spectrometry (LAMIS); Filamentation; Molecular Emission Spectra.

1. Introduction

Laser Induced Breakdown Spectroscopy (LIBS) is a powerful direct solid sampling analytical techniquefor rapid, all-optical elemental analysis of materials. The process involves a high-power pulsed laser beam directed and focused onto a sample surface to instantaneously convert a finite volume of the sample into plasma (laser ablation),and subsequent analysisof the resulting optical emission spectra. One of the advantages of LIBS is its all-optical nature, which enablesstand-off elemental analysis. The most common configuration for creating the laser induced plasma at a distance is by focusing high energy nanosecond laser pulses with large open-truss telescope systems.[1,2]One of the challenges with using nanosecond (ns) lasers for stand-off LIBS is the limited operation range, associated with difficulty to tightly focus the laser beam at long distances. Classical optical diffraction causes the laser beam diameter at the focus to linearly increase with focusing distance, and as a result, delivering sufficient laser fluence for ablation at a distance is challenging. Today, conventional ns LIBS stand-off material analysis [1,2]is limited to a little over 100 meters.[3]

In contrast to nanosecond lasers, it is possible for femtosecond laser beams to propagate over long distances as a result of the non-linear process of laser filamentation.[4]Filamentation of an intense, ultrashort laser pulse arises from dynamic balance between beam Kerr self-focusing and defocusing action of free electrons produced by multi-photon ionization of air molecules.[4–7]Unlike ns lasers, self-sustained fs filaments do not require large telescope systems to focus the laser beam. Filaments have a central core (typical diameter: 10^2 μm) with high intensity (10^{13} W/cm^2[8]) that is surrounded by an energy reservoir, which can replenish the

filament core and support the filamentationprocess over long distances.The propagation distance before filament formation and the filament length depend on the laser parameters, and can be formed with pre-focused or freely propagating femtosecond laser beams.[9]Remote filament induced breakdown spectroscopyhas been previously reported for elemental discrimination of composite graphite samples,[10] biological materials[11,12], metals[13] detection and sensing of explosives.[14]

The ability to perform not just elemental analysis but also isotopic analysis at a distance is important for some remote sensing applications, including nuclear non-proliferation and forensics.[15,16]Despite all the research on LIBS, the ability to provide isotopic information is limited toonly a few studies (e.g., H, Li and U).[17–19]The recent development of Laser Ablation Molecular Isotopic Spectrometry (LAMIS) introduced a new way for direct isotopic analysis at atmospheric pressure. LAMIS uses radiative transitions from molecular species either directly vaporized from a sample or formed by associative mechanisms of atoms or ions in a laser ablation plume,[20,21] thereby expanding all the advantages of LIBS to isotopic analysis.LAMISanalysis of several isotope systems(H/D, $^{10/11}$B, $^{12/13}$C, $^{86/87/88}$Sr, $^{90/91/92/94}$Zr) has been reported[18,22–25]using conventional nanosecond and femtosecond laboratory instruments involving short focal length lenses.

In this work, we introduce a new technology, Femtosecond Filament-Induced Laser Ablation Molecular Isotopic Spectrometry (F^2-LAMIS), which enables real-time isotopic analysisat remote distances.We demonstrate that the stable filaments generated by high-power,ultrashort laser pluses can be used for stand-off isotopic analysis of Zr, which contains five stable isotopes. The filament-inducedplasma characteristics and F^2-LAMIS

spectrawere studied as a function of filament propagation distance. Spectral fitting of F^2-LAMIS spectra was incorporated for semi-quantitative isotopic ratio measurements of Zr as a function of distance.

2. Experimental system

A Ti:Sapphire(800 nm) femtosecond laser system (Mai-Tai oscillator coupled to a TSA-25 amplifier, Spectra Physics) was used for filament generation, delivering 100 fs, 7mJ pulses at a repetition rate of 10Hz. Filamentswere generated by focusing the femtosecond laser beam with a plano convex lens (f = 5 m)(**Fig. 1**). The laser filaments propagated over several meters up to a distance of 7.8 m which was the limit of the available laboratory space.The filament propagation was clearly visible in reduced light conditions, extending over several meters, well beyond the calculated Rayleigh length of the focused laser beam (0.25 m).A schematic of the experimental system is shown in **Fig.1**.

A zirconium (Zr) metalplate (99.2%, Alfa Aesar) was used as a sample.The Zr samplewas placed on a motorized yz micrometric stage which was mounted onmoveable carrier base alongan optical rail,which was aligned parallel to the filament propagation direction. The distance between the lens and the sample (filament propagation distance-x) was controlled by translating the carrier on the rail. An iris with variable diameter was placed 5 cm in front the sample to ensure that the alignment was maintained for all sample positions along the rail. The iris remained open (diameter >1 cm) during the emission and acoustic measurements, ensuring that the energy reservoir surrounding the filament core was not blocked or influenced by the iris.[26]

The filament-induced plasma from the Zr sample was imaged onto a collection fiber by using a plano-convex lens (*f*=5 cm). The fiber was connected to the entrance slit of a Czerny-Turner spectrometer (focal length = 1.25 m, Horiba JY 1250M) equipped with an intensified charge-coupled device (ICCD) (PI MAX 1024, Princeton Instruments) for spectral acquisition. The grating of the spectrometer had agroove density of 3600 per mm. The instrumentalresolution of the spectrometer was determined as 11.8 pm at 435.8 nm,by using a mercury lamp.An acoustic signal sensor connected to an oscilloscope, was used to record acoustic signals in the filament-induced plasma vicinity. Both the spectral emission collection optics and fiber system, and the acoustic sensor were directly mounted on the sample carrier base, to ensure that the collectionremained unaffected as a function of filament propagation distance.

The sample was translated along the vertical axis at a constant translation speed of 0.02 mm/s, thereby forming craters on the Zrplate surface. Following ablation, the three dimensional morphology of the ablated craters was measured by using a white light interferometer (ZygoNewView 6K).

3. Results and discussion

3.1 F^2-LAMIS spectra and spectraldeconvolution

The spectral range of 461.90 to 463.70 nm was selected for spectroscopic analysis of the filament-induced plasma, covering theα(0,0) band the of $d\,^3\Delta_3 - a\,^3\Delta_3$ system of ZrO andfour zirconium atomic lines (Zr I 462.64 nm/462.77 nm/463.40 nm/463.46 nm).[25]**Fig.2a** shows the plasma spectral emission at a filament propagation distance of 6.8 m. In order to reconstruct the

molecular and atomic emission from the acquired spectra, a fitting procedure was implemented(**Fig. 2b**).The observed transitions in diatomic molecules can be calculated by: $\Delta E = E(e^{'}, v^{'}, J^{'}) - E(e^{''}, v^{''}, J^{''})$, where $E(e, v, J) = E_{elc}(e) + E_{vib}(e, v) + E_{rot}(e, v, J)$. E_{elc} , E_{vib} and E_{rot} are the electronic, vibrational and rotational quantum states. The intensity was determined by the transition probability and the population of the excited state $E(e^{'}, v^{'}, J^{'})$. A detailed description of the fitting procedure can be found in our previous work.[20,25]For the simulation, molecular parameters reported by Kaledin*et al.*[27]were used,and the peak profile of atomic lines was assumed to bea Lorentzianfunction.

Using this fitting procedure, the components of ZrO molecular band and four Zratomic lines were reconstructed,and are shown together with the experimental spectra in **Fig.2c**. The intensity of the ZrO molecular emission is comparable to the zirconium atomic emission.The rotational structure in the ZrOspectra is clearly resolved. Typical residual (difference between experimental and fitted data)at each wavelength was less than 6% (**Fig.2d**),with a distribution that was independent of wavelength, thereby demonstrating that this fitting procedure allows for high precision molecular band and atomic linecomponentdeconvolution.

3.2 Characterization of filament-induced plasmas at different propagation distances

In order to characterize the optical emission of plasmas generated at different filament propagationdistances, we studied the intensity variation of the zirconium oxide molecular band (α(0,0) band of the $d\,^3\Delta_3 - a\,^3\Delta_3$ system) and the zirconium atomic line (Zr I 462.64 nm). The acoustic signal and excitation temperature also were measured. The vibrational bandhead intensity was used as the emission signal of the ZrO molecules.

The atomic and molecular emission intensities, acoustic signals and plasma temperaturesas functions of filament propagation distancesare shown in **Fig.3**.The intensities of both ZrO and Zr I initially increase with filament propagationdistance before reachinga maximum at a distance of 6.8 m. Following that,they gradually decrease to about 70% of the maximal intensity at a filament propagation distance of 7.8 m (**Fig.2a**). Dueto limitations in available experimental space, the emission of the plasma generated after 7.8 m could not be measured.

Acoustic signals provide a versatile method for monitoring the general strength of filament-induced plasma, and have been used in the past to monitor the laser ablation threshold[28] or to correct for shot-to-shot analyte emission variations.[29]Higher acoustic signal typically indicates that stronger plasma is generated.**Fig. 3b** shows the variation of acoustic signal over distance,exhibiting behavior similarto that of the plasma emission intensity. For the plasma excitation temperature measurements as a function of filament propagation distance, we used the two zirconium atomic lines (Zr I 463.40 nm and 462.64 nm) in the Boltzmann Plot method.[30]Unlike emission and acoustic signal intensity, the excitation temperature showeda gradual increase with filament propagation distance (**Fig. 3c**).

The variation of atomic and molecular intensity, as well as acoustic signal, as a function of filament propagation distance, can be attributed to two main factors: excitation temperature and ablated mass variation. First, we investigated the dependence of the Zr I line intensity over plasma temperature.Treating the plasma as homogeneous and in thermal equilibrium, we calculatedthe contribution of temperature variations on the signal intensity. Both the ionization equilibrium, which follows the Saha equation, and the

electron population,which follows Boltzmann equilibrium,wereused. For anelectron density,n_e = 10^{17}-10^{18} cm^{-3}, the maximum variation of relative spectral emission intensity (ΔI) of Zr I 462.64 nm at different filament propagation distances, attributed to temperature changes,is:ΔI=27.8-28.6%. However, the experimental variation of Zr I 462.64 nm intensities as a function of filament propagation distance can be up to 70%, which indicates that the second contributing factor, ablated mass,may vary with filament propagation distance.

Fig.4shows the depth profiles of filament-ablated craters at four selected propagation distances, which correspond to the optical focal point of the lens (5 m), the half maximum (6.0 m) and maximum (6.8 m) of the plasma emission intensity, and the maximum distance (7.8 m). Each depth profile was obtained by averaging all individual pixels in the white light interferometry three-dimensional sample morphology image. **Fig.4(a)**shows that although the diameters of the craters obtained at the four distances are similar (~450 μm), their depths are quite different.Dynamic energy redistribution along the filament path may directly affect the ablation efficiency characteristics. Deepest craters werecreated at a filament propagation distance of 6.8 m, which indicates that the laser intensity in the filament corewas the highest in that position. The ablated volume was measured by spatial integration of the crater profiles, which was in turn used to calculate the relative ablated mass as a function of filament propagation distance (**Fig.4b)**. Correlations between the ablated mass and intensities of the Zr I line and ZrO molecular bandat different distances are shown in **Fig.3a**.

In order to further characterize the emission and physical characteristics of the plasma generated at different filament propagationdistances, we studied the temporalbehavior of

the zirconium atomic emission, ZrO molecular emissionand plasma excitation temperature (**Fig.5)**. For the zirconium atomic lines, the intensity decreases with time, a behavior which is commonly observedin laser induced plasmas.In contrast, the molecular emission intensity initially increases with delay time and reachesits maximumat 500 ns, following which, it decays with time. The different behavior between the atomic and molecular emissionmay be attributed to the fundamentally different plasma conditions that are required for ZrOmolecule formationvia the combination of zirconium and oxygen atoms. Figs. 5a and 5b show that both Zr I line and ZrO band emissions were stronger at distances over 6.0 m than those at 5.0 m. The plasma generated at the lens focal distance (5.0 m) hasslightly lowertemperaturecompared to that of the plasma generated at 6.0, 6.8 and 7.8 m. The temporal evolution of the excitation temperature for the plasmas generated at 6.8 and 7.8 m is very similar for all detection gate delays, in agreement with the temporally integrated mean excitation temperature shown in **Fig.3**.

3.3Isotopic analysis with F^2-LAMIS

The zirconium sample used in this work had natural isotopic abundance (^{90}Zr:^{91}Zr:^{92}Zr:^{94}Zr:^{96}Zr=2.96:0.65:0.99:1:0.16).[31]Our previous report[25] showed that isotopic information can be obtained by analyzing the (0,1) and (1,0) ZrO molecular bandsof $E\,^1\Sigma^+ - X\,^1\Sigma^+$ and $d\,^3\Delta - a\,^3\Delta$systems and that the α(0,1) band of the $d\,^3\Delta_3 - a\,^3\Delta_3$ system is optimal for zirconium isotopic analysis. **Fig.6a**shows the typical spectra acquired at filament distances of 5.0, 6.0. 6.8 and 7.8 m. The ICCD gate delay and gate width were 3 μs and 20 μs respectively, and were optimized in order to improve the signal-to-noise ratio of the isotopic signatures.Molecular band intensities and

interferences from nearby zirconium atomic and ionic lines were taken into account during the optimization process.As shown in **Fig.6a,** four different isotopic zirconium oxide molecular bands, i.e.^{90}ZrO, ^{91}ZrO, ^{92}ZrO and ^{94}ZrO,were clearlyresolved. The molecular band of ^{96}ZrO could not be assigned with certainty due to the low concentration of ^{96}Zr in the sample that results in a weak emission line. The weak ^{96}ZrO is, in addition, interfered with noise and rotation structure of other molecular bands nearby.[32]The ratio of zirconium isotopes can be deduced by fitting of experimental to the theoretical spectra of the α(0,1) band of the $d\,^3\Delta_3 - a\,^3\Delta_3$ system, as demonstrated in our previous work.[25]**Fig.6b**shows the deduced isotope ratios of ^{90}Zr/^{94}Zr, ^{91}Zr/^{94}Zr and ^{92}Zr/^{94}Zr as a function of filament propagation distance. Although these isotope ratios deviate from the true isotopic composition of the sample, each isotope ratio remainsfairly constantwith filament propagation distance. As with any analytical technique, more accurate quantitative analysis is expected with the use of standard samples for calibration. These results indicate that the influence of the filament propagation distance on quantification is minimal, and that F^2-LAMIS can be a powerful and versatile technology for remote semi-quantitative isotopic analysis.

4. Conclusions

We introduced a new laser technology, F^2-LAMIS, which enables all-optical isotope analysis at remote distances, through the combination offs laser filamentation and ablation-based molecular isotopic spectroscopy. We demonstrated the first experimental measurement of isotopes with F^2-LAMIS at distances up to 7.8 m.The plasma properties and the dependence of both molecular and atomic Zremission over filament propagation

distance were investigated. Spectral fitting of F^2-LAMIS spectra allowed semi-quantitiveisotopic ratio analysis, thereby minimizing the need for standards. This spectral-fitting approach is also applicable to other elements. For example, molecular bands with appreciable isotope shifts have been experimentally observed for boron and carbon. This technology, combined with a large diameter telescope for collection of plasma emission, can be used for isotopicanalysis at remote distances, in applications ranging from nuclear non-proliferation to environmental research. For standoff plasma ablation, femtosecond laser filament offers an advantage over nanosecond laser in delivering laser energy with high fluence. A major challenge for determination at extended standoff distances is collection of plasma emission as the solid angle of light collection decreases in a quadratic fashion to the distance between the plasma and telescope. One possible solution to improve the standoff plasma emission collection efficiency is through the use of the filament self-created long-lived optical waveguides,[33]in which lifetimes were reported to be up to millisecond; clearly, more work needs to be done to evaluate such possibility and its performance.

Acknowledgement

The research was supported by the US Department of Energy, Office of Nuclear Nonproliferation and Office of Basic Energy Sciences,under contract number DEAC02-05CH112 at the Lawrence Berkeley National Laboratory.

References:

[1] C. López-Moreno, S. Palanco, J. Javier Laserna, F. DeLucia Jr, A.W. Miziolek, J. Rose, et al., Test of a stand-off laser-induced breakdown spectroscopy sensor for the detection of explosive residues on solid surfaces, J. Anal. At. Spectrom. 21 (2006) 55–60.

[2] I. Gaona, P. Lucena, J. Moros, F.J. Fortes, S. Guirado, J. Serrano, et al., Evaluating the use of standoff LIBS in architectural heritage: surveying the Cathedral of Málaga, J. Anal. At. Spectrom. 28 (2013) 810–820.

[3] J.J. Laserna, R.F. Reyes, R. González, L. Tobaria, P. Lucena, Study on the effect of beam propagation through atmospheric turbulence on standoff nanosecond laser induced breakdown spectroscopy measurements, Opt. Express. 17 (2009) 10265–10276.

[4] M. Rodriguez, R. Bourayou, G. Méjean, J. Kasparian, J. Yu, E. Salmon, et al., Kilometer-range nonlinear propagation of femtosecond laser pulses, Phys. Rev. E - Stat. Nonlinear, Soft Matter Phys. 69 (2004) 1–7.

[5] M. Scheller, M.S. Mills, M.-A. Miri, W. Cheng, J. V. Moloney, M. Kolesik, et al., Externally refuelled optical filaments, Nat. Photonics. 8 (2014) 297–301.

[6] S.L. Chin, T.-J. Wang, C. Marceau, J. Wu, J.S. Liu, O. Kosareva, et al., Advances in intense femtosecond laser filamentation in air, Laser Phys. 22 (2012) 1–53.

[7] M. Durand, A. Houard, B. Prade, A. Mysyrowicz, A. Durécu, B. Moreau, et al., Kilometer range filamentation, Opt. Express. 21 (2013) 26836–26845.

[8] A. Brodeur, C.Y. Chien, F.A. Ilkov, S.L. Chin, O.G. Kosareva, V.P. Kandidov, Moving focus in the propagation of ultrashort laser pulses in air, Opt. Lett. 22 (1997) 304–306.

[9] Z. Hao, J. Zhang, Z. Zhang, X. Yuan, Z. Zheng, X. Lu, et al., Characteristics of multiple filaments generated by femtosecond laser pulses in air: Prefocused versus free propagation, Phys. Rev. E. 74 (2006) 066402.

[10] E.J. Judge, G. Heck, E.B. Cerkez, R.J. Levis, Discrimination of composite graphite samples using remote filament-induced breakdown spectroscopy, Anal. Chem. 81 (2009) 2658–2663.

[11] H.L. Xu, G. Méjean, W. Liu, Y. Kamali, J.-F.F. Daigle, A. Azarm, et al., Remote detection of similar biological materials using femtosecond filament-induced breakdown spectroscopy, Appl. Phys. B Lasers Opt. 87 (2007) 151–156.

[12] P. Rohwetter, K. Stelmaszczyk, L. Wöste, R. Ackermann, G. Méjean, E. Salmon, et al., Filament-induced remote surface ablation for long range laser-induced breakdown spectroscopy operation, Spectrochim. Acta Part B At. Spectrosc. 60 (2005) 1025–1033.

[13] K. Stelmaszczyk, P. Rohwetter, G. Méjean, J. Yu, E. Salmon, J. Kasparian, et al., Long-distance remote laser-induced breakdown spectroscopy using filamentation in air, Appl. Phys. Lett. 85 (2004) 3977–3979.

[14] D. Mirell, O. Chalus, K. Peterson, J.-C. Diels, Remote sensing of explosives using infrared and ultraviolet filaments, J. Opt. Soc. Am. B. 25 (2008) B108–B111.

[15] G.R. Krishna, H.R. Ravindra, B. Gopalan, S. Syamsunder, Determination of iron in nuclear grade zirconium oxide by x-ray fluorescence spectrometry using an internal intensity reference, Anal. Chim. Acta. 309 (1995) 333–338.

[16] A. Simonists, F. Corte, A. Wispelaere, J. Hoste, Nuclear data measurements for zirconium isotopes used for activation analysis and neutron metrology, J. Radioanal. Nucl. Chem. Artic. 113 (1987) 187–197.

[17] G.C.-Y. Chan, X. Mao, I. Choi, A. Sarkar, O.P. Lam, D.K. Shuh, et al., Multiple emission line analysis for improved isotopic determination of uranium – a computer simulation study, Spectrochim. Acta Part B At. Spectrosc. 89 (2013) 40–49.

[18] A. Sarkar, X. Mao, G.C.Y. Chan, R.E. Russo, Laser ablation molecular isotopic spectrometry of water for 1D2/1H1 ratio analysis, Spectrochim. Acta - Part B At. Spectrosc. 88 (2013) 46–53.

[19] D. Cremers, A. Beddingfield, R. Smithwick, R.C. Chinni, C.R. Jones, B. Beardsley, et al., Monitoring uranium, hydrogen, and lithium and their isotopes using a compact laser-induced breakdown spectroscopy (LIBS) probe and high-resolution spectrometer, Appl. Spectrosc. 66 (2012) 250–261.

[20] R.E. Russo, A. Bol'shakov, X. Mao, C.P. McKay, D.L. Perry, O. Sorkhabi, Laser Ablation Molecular Isotopic Spectrometry, Spectrochim. Acta Part B At. Spectrosc. 66 (2011) 99–104.

[21] X. Mao, A. Bol'shakov, D.L. Perry, O. Sorkhabi, R.E. Russo, Laser Ablation Molecular Isotopic Spectrometry: Parameter influence on boron isotope measurements, Spectrochim. Acta Part B At. Spectrosc. 66 (2011) 604–609.

[22] X. Mao, A.A. Bol'Shakov, I. Choi, C.P. McKay, D.L. Perry, O. Sorkhabi, et al., Laser Ablation Molecular Isotopic Spectrometry: Strontium and its isotopes, Spectrochim. Acta - Part B At. Spectrosc. 66 (2011) 767–775.

[23] M. Dong, X. Mao, J.J. Gonzalez, J. Lu, R.E. Russo, Carbon isotope separation and molecular formation in laser-induced plasmas by laser ablation molecular isotopic spectrometry, Anal. Chem. 85 (2013) 2899–2906.

[24] P. Ko, I. Jovanovic, Boron isotopic measurements from spectrally filtered non-gated molecular spectra induced by laser ablation, Spectrochim. Acta Part B At. Spectrosc. 90 (2013) 68–71.

[25] H. Hou, G.C.-Y. Chan, X. Mao, V. Zorba, R. Zheng, R.E. Russo, Femtosecond laser ablation molecular isotopic spectrometry for zirconium isotope analysis, Anal. Chem. 87 (2015) 4788–4796.

[26] W. Liu, F. Théberge, E. Arévalo, J.F. Gravel, A. Becker, S.L. Chin, Experiment and simulations on the energy reservoir effect in femtosecond light filaments, Opt. Lett. 30 (2005) 2602–2604.

[27] L.A. Kaledin, J.E. Mccord, M.C. Heaven, Laser Spectroscopy of ZrO: Accurate Term Energies for the Triplet States, J. Mol. Spectrosc. 174 (1995) 93–99.

[28] D.J.O. Orzi, F.C. Alvira, G.M. Bilmes, Determination of femtosecond ablation thresholds by using laser ablation induced photoacoustics (LAIP), Appl. Phys. A. 110 (2012) 735–739.

[29] A. Hrdlička, L. Zaorálková, M. Galiová, T. Čtvrtníčková, V. Kanický, V. Otruba, et al., Correlation of acoustic and optical emission signals produced at 1064 and 532 nm laser-induced breakdown spectroscopy (LIBS) of glazed wall tiles, Spectrochim. Acta Part B At. Spectrosc. 64 (2009) 74–78.

[30] M. Baudelet, C.C.C. Willis, L. Shah, M. Richardson, Laser-induced breakdown spectroscopy of copper with a 2 microm thulium fiber laser, Opt. Express. 18 (2010) 7905–7910.

[31] M. Berglund, M.E. Wieser, Isotopic compositions of the elements 2009 (IUPAC Technical Report), Pure Appl. Chem. 83 (2011) 397–410.

[32] M. Afaf, Singlet systems of zirconium oxide, Astrophys. J. 314 (1987) 415–418.

[33] N. Jhajj, E.W. Rosenthal, R. Birnbaum, J.K. Wahlstrand, H.M. Milchberg, Demonstration of Long-Lived High-Power Optical Waveguides in Air, Phys. Rev. X. 4 (2014) 11027.

Figure Captions

Fig. 1 Schematic diagram of the F^2-LAMIS experimental setup.

Fig. 2 (a) Typical F^2-LAMIS spectrum acquired from the Zr target at a filament propagation distance of 6.8 m. (b) The molecular band and atomic lines were re-constructed through a fitting procedure. (c) Fitted and experimental spectra. The fitting residual is shown in (d). The ICCD gate delay and gate width were set at 1.5 μs and 10 μs, respectively.

Fig. 3 Variations of the emission intensity of the ZrO molecular bandhead and Zr I 462.64 nm (a), acoustic signal (b), and plasma excitation temperature (c) as a function of filament propagation distance. The error bar represents the standard deviation of 10 separate measurements. Each measurement is an accumulation of 64 laser shots. For spectral acquisition, the ICCD gate delay and gate width were set at1.5 μs and 10 μs, respectively.

Fig. 4 (a) Femtosecond filament ablatedcraters on the zirconium metal target at different filament propagation distances (5.0, 6.0, 6.8 and 7.8 m), and (b) comparison of the relative ablated mass.The sample translation speed was 0.02 mm/s.

Fig. 5 Temporal evolution of the (a) Zr I 462.64 nm intensity, (b) ZrO molecular band head intensity and (c) excitation temperature of plasmas generated at filament propagation distances of 5.0, 6.0, 6.8 and 7.8 m.

Fig. 6 (a) Typical spectra of the ZrOα(0,1) band of the $d\,^3\Delta_3 - a\,^3\Delta_3$ system obtained at different filament propagation distances. The ICCD gate delay was 3 μs and the gate width was 20 μs. Each spectrum was the average of 500 laser shots. (b)Deduced atomic ratios of $^{90}Zr/^{94}Zr$, $^{91}Zr/^{94}Zr$ and $^{92}Zr/^{94}Zr$ as a function of filament propagation distance. Error bars represent the standard deviation of 10 measurements.

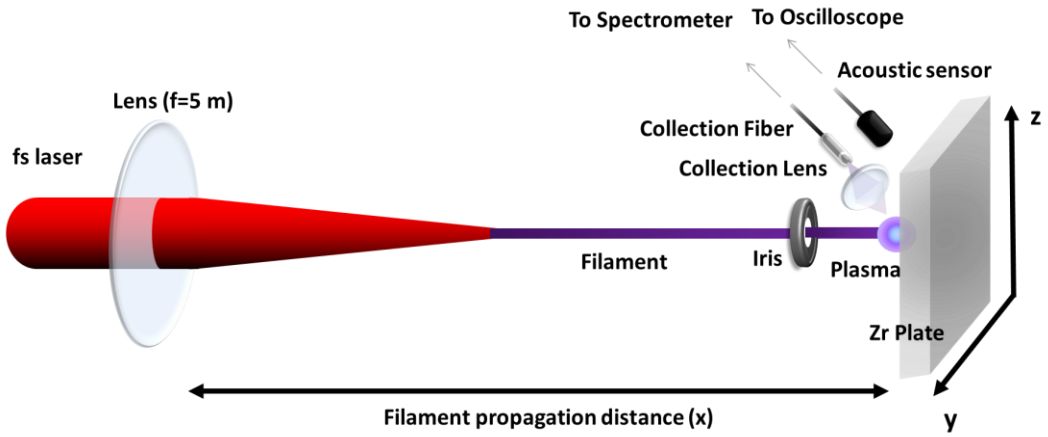

Fig. 1 Schematic diagram of the F^2-LAMIS experimental setup.

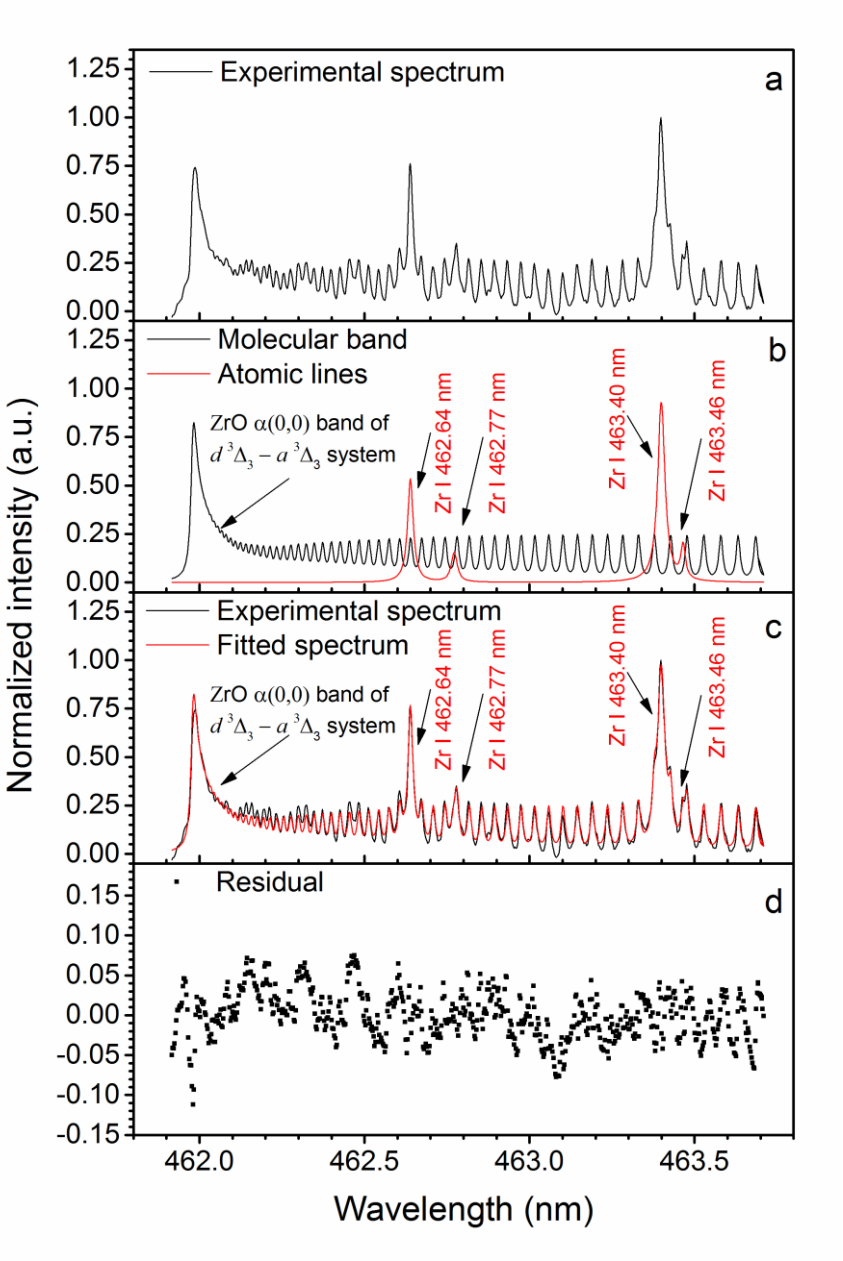

Fig. 2 (a) Typical F^2-LAMIS spectrum acquired from the Zr target at a filament propagation distance of 6.8 m. (b) The molecular band and atomic lines were re-constructed through a fitting procedure. (c) Fitted and experimental spectra. The fitting residual is shown in (d).The ICCD gate delay and gate width were set at 1.5 μs and 10 μs, respectively.

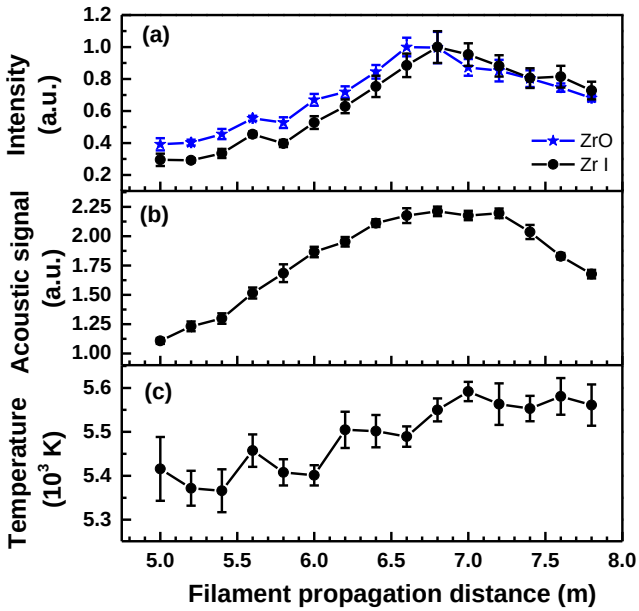

Fig. 3. Variations of the emission intensity of the ZrO molecular bandhead and Zr I 462.64 nm (a), acoustic signal (b), and plasma excitation temperature (c) as a function of filament propagation distance. The error bar represents the standard deviation of 10 separate measurements. Each measurement is an accumulation of 64 laser shots. For spectral acquisition, the ICCD gate delay and gate width were set at1.5 μs and 10 μs, respectively.

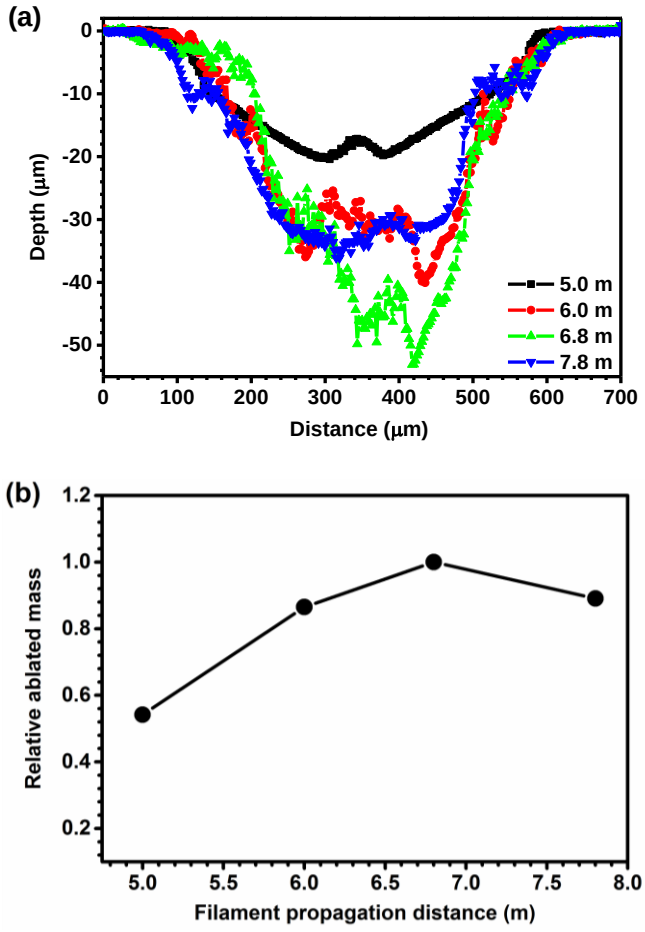

Fig. 4 (a) Femtosecond filament ablated craters on the zirconium metal target at different filament propagation distances (5.0, 6.0, 6.8 and 7.8 m), and (b) comparison of the relative ablated mass. The sample translation speed was 0.02 mm/s.

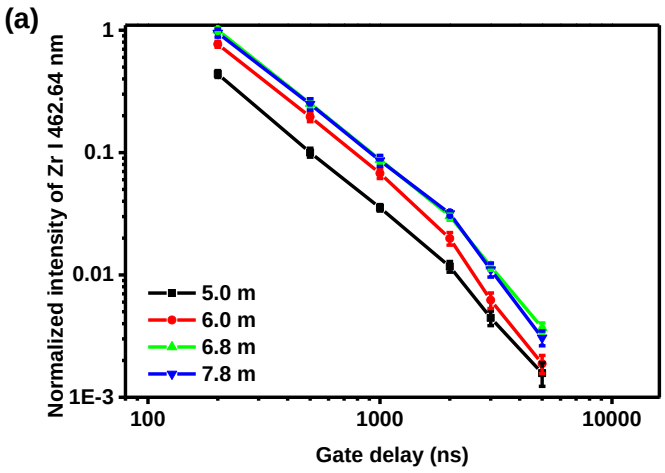

1

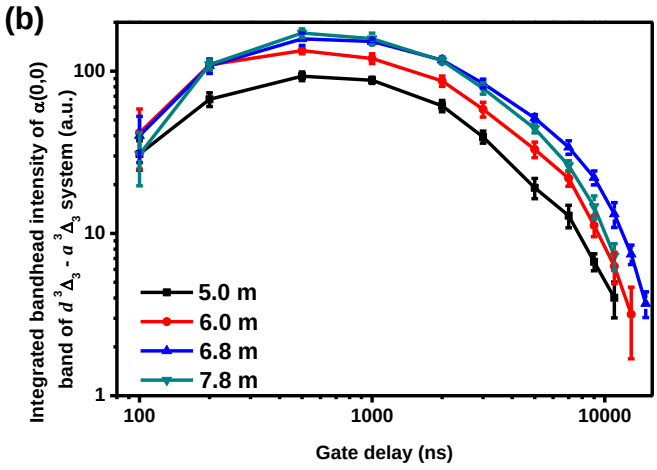

2

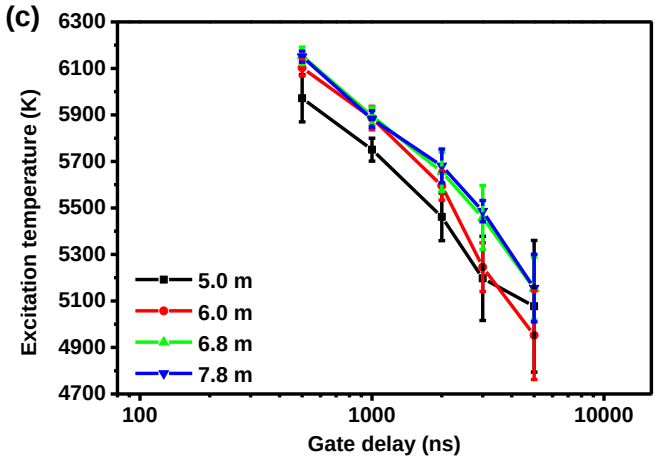

3

4 Fig. 5 Temporal evolution of the (a) Zr I 462.64 nm intensity, (b) ZrO molecular
5 band head intensity and (c) excitation temperature of plasmas generated at
6 filament propagation distances of 5.0, 6.0, 6.8 and 7.8 m.

7

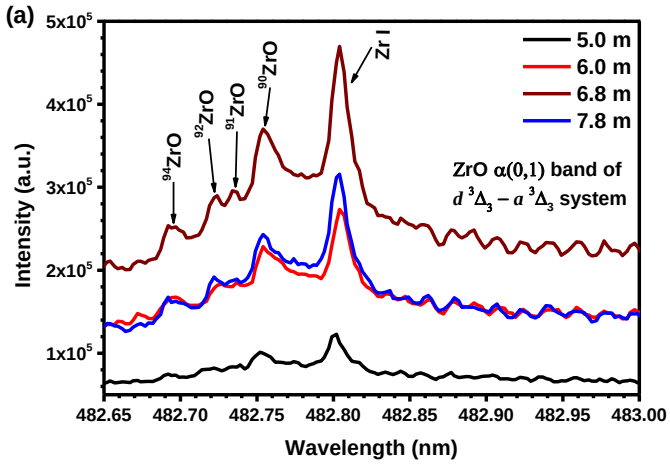

Fig. 6 (a) Typical spectra of the ZrOα(0,1) band of the $d\,^3\Delta_3 - a\,^3\Delta_3$ system obtained at different filament propagation distances. The ICCD gate delay was 3 μs and the gate width was 20 μs. Each spectrum was the average of 500 laser shots. (b) Deduced atomic ratios of ^{90}Zr/^{94}Zr, ^{91}Zr/^{94}Zr and ^{92}Zr/^{94}Zr as a function of filament propagation distance. Error bars represent the standard deviation of 10 measurements.